Hydrodynamics of the collapse of a laser-heated and -compressed microballoon

Z. Ahmad,[1] Yu. A. Zakharenkov, I. G. Lebo, T. V. Mishchenko,[2]
V. B. Rozanov, T. A. Hall,[1] A. S. Shikanov, and G. V. Shpatakovskaya[2]

P. N. Lebedev Physics Institute, Academy of Sciences of the USSR, Moscow;[1] University of Essex, United Kingdom; [2] Institute of Applied Mathematics, Academy of Sciences of the USSR, Moscow

Measurements of the spectra of the neutral atoms of spherical shell targets heated and compressed by laser light at the Vulcan installation (in the United Kingdom) are reported. The observed spectra are broader than the calculated spectra. This difference indicates the onset of turbulent mixing in the target. The double-humped structure of the spectrum in the case of a nonuniform irradiation implies the formation of jets.

INTRODUCTION

In experiments on the laser heating and compression of shell targets,[1] two characteristic stages can be distinguished in the evolution of the compressed microballoons. The first extends to the end of the heating laser pulse and usually lasts no longer than the target compression time. During this stage, a hot plasma (with a temperature of 1 keV or higher) with an ion density $\eta_i \sim 10^{20}$–10^{22} cm^{-3} is produced at the surface of the microballoon which is being accelerated toward its center. This plasma typically moves at a velocity in the range $(4$–$8) \cdot 10^7$ cm/s. As has been shown theoretically[2,3] and confirmed experimentally,[4-6] recombination of ions to a neutral state in the moving plasma corona is improbable. Such recombination is possible only on the slow tail of the velocity distribution (at velocities below $4 \cdot 10^7$ cm/s). For this reason, ion mass spectroscopy has been adopted widely for studying the hydrodynamic processes (the flow of mass, the ablation pressure of the laser-heated target, the hydrodynamic efficiency, etc.).[7]

The second stage in the emission of target material begins at the instant at which the target collapses at the center. If the parameters of the laser pulse are matched with those of the target, the heating of the plasma by the laser light has come to a halt by this time. In this case the typical velocities and charge composition depend on the energy deposited in the target and on the density and temperature of the compressed matter. For example, the central pressure can exceed $P \sim 10^9$ bar at the densities ($\rho \approx 10$–100 g/cm^3) and temperatures ($T \approx 10$–100 eV) typical of recent experiments,[8] and the velocity can exceed the characteristic sound velocities for these values:

$$v \gtrsim \left(\frac{5}{3} \frac{p}{\rho} \right)^{1/2} \simeq 10^7 \text{ cm/s}.$$

In the collapsing material, the ions are accompanied by a certain number of neutral atoms, which have been formed by recombination during the collapse.[9] The relative number of such atoms evidently increases with increasing density and decreasing temperature in the compressed target.

It was shown in Ref. 10 by numerical calculations that in experiments with matched targets and moderate light flux densities [specifically, for $q\lambda^2 \lesssim 10^{14}$ (W/cm^2)·μm^2, where q is the light intensity and λ is the wavelength] the neutral component can constitute 90% of the mass of the compressed shell. It follows that one can develop a particle-based

diagnostic procedure for diagnostics of compressed microballoons—for determining the hydrodynamic efficiency, the unevaporated target mass, and other important properties.

EXPERIMENTAL APPARATUS

The experiments were carried out at the Vulcan laser installation at the Rutherford Appleton laboratory in the United Kingdom.[11] This installation has 12 beams; the wavelength of the laser light is 0.53 μm; and the laser energy is 800 J in a pulse 0.6 ns long. High-aspect-ratio glass shell targets, 500–700 μm in diameter with a wall thickness of 0.75–1.3 μm, were used. These targets were filled with a deuterium-tritium mixture to a pressure of 2–3 atm. Several shots were carried out on hollow microballoons of glass (with a wall thickness of 1.5–2.5 μm) and of polystyrene (250–400 μm in diameter, with a thickness to 11 μm). The purpose of these experiments was to study how the laser-beam focusing conditions affect the characteristics of the compression.[12]

The diagnostic apparatus at this installation includes x-ray apparatus, neutron and α-particle detectors,[13] and devices which detect the fluxes of neutral atoms.[14] In the experiments, the results of measurements obtained when the light was focused on the rear surface of the shell (the diameter of the laser beam at the front surface of the target was 200 μm) were compared with the results obtained when the focusing was smoothed by special miniature phase plates in the laser beams.

The axis along which the particle fluxes were observed passed through the center of the equilateral triangle created on the target surface by the three closest laser beams (the angular distance to the axis of the nearest laser beam was 30°). This arrangement made it possible to detect the ions and atoms emitted from a "cold" target region surrounded by three "hot" regions.

An annular ion collector was positioned in a drift tube 90 cm from the target (Fig. 1). An electron multiplier was positioned behind it, at a point 110 cm from the target. An electrostatic ion deflector (with a potential difference up to 3 kV and a slit width of 0.4 cm) was placed between the collector and the electron multiplier to remove ions from the atomic beam.

EXPERIMENTAL RESULTS

Figure 2 shows oscilloscope traces of the output signals from the collector and the electron multiplier for shots with
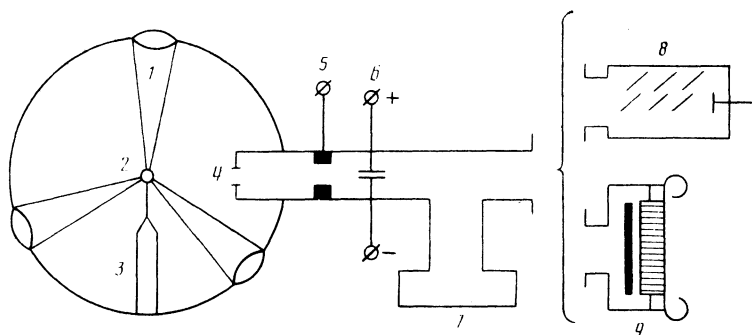
FIG. 1. Experimental layout. 1—Laser beam; 2—target; 3—target holder; 4—entrance diaphragm of atomic-beam diagnostic channel; 5—ion collector; 6—ion deflector; 7—vacuum pump; 8—electron multiplier; 9—microchannel framing image-converter camera.

"sharp focusing" (Fig. 2a) and with "smoothed" irradiation of the target (Fig. 2b).

Analysis of traces of this sort shows that a double structure of the ion signal is characteristic of nonuniform irradiation. The first ion peak (Fig. 2a) corresponds to a velocity of $8.2 \cdot 10^7$ cm/s. This peak is formed by ions emitted by the hot regions on the target surface. The second ion peak has a velocity of $3.8 \cdot 10^7$ cm/s, which corresponds to the cold region on the microballoon. Note that there are slow ions (with velocities to $1.5 \cdot 10^7$ cm/s) in the case of a nonuniform irradiation.

Neutral atoms were detected with velocities in the range $(0.7–4.4) \cdot 10^7$ cm/s. In the case of the nonuniform irradiation, a group of atoms with velocities of $(3–4) \cdot 10^7$ cm/s was clearly detected (Fig. 2a). The smooth irradiation is characterized by a rounded maximum on the current signal at $v \sim (1.2–1.5) \cdot 10^7$ cm/s, whose decay is steeper than in the case of shots with nonuniform irradiation.

Additional, and important, information on the emission of neutral atoms was obtained in experiments with particle pinhole cameras. These cameras had holes 50 and 100 μm in diameter, at distances of 5–25 cm from the target. The particle beams which formed the image of the source passed through an electrostatic deflector and were detected by a microchannel image-converter camera; a pulsed voltage was applied to the microchannel plate.[15] By adjusting the delay (3–8 μs) of the arrival of the high-voltage pulse with respect to the time of emission, and by adjusting the duration of this pulse (2–8 μs), we were able to record images (frames) in a given interval of atomic velocities.

Figure 3 shows a pinhole photograph of a polystyrene shell with an initial diameter of 266 μm and a thickness of 9.2 μm. The multichannel detector was strobed at a rate corresponding to velocities of $(1.3–1.8) \cdot 10^7$ cm/s. It can be seen from Fig. 3 that the slow atoms which are detected are emit-

ted not only by the target but also by the target holder (a glass capillary). This emission of atoms from the holder could result from heating of the holder as a result of heat transfer from the target (this transfer could include radiative transfer) and also from a possible incidence of laser light, especially since the target had small dimensions, and the laser energy was high ($E_L = 748$ J). A photodensitometer study of the target image in an axial cross section (Fig. 3b) revealed spatial structure in the particle source with a resolution $\sim 150 \mu$m. This resolution corresponds to a geometric-optics estimate (the hole diameter of the pinhole camera was $\sim 100 \mu$m, and the gain was 10).

RESULTS OF NUMERICAL CALCULATIONS

The laser heating, compression, and expansion of a shell target were modeled in calculations carried out with the one-dimensional DIANA program.[10,16] It was assumed in these calculations that the laser energy was absorbed completely. The laser pulse had a temporal shape

$$\frac{dE}{dt} = \dot{E}_0 \exp\left[-4 \ln 2\left(\frac{t-t_0}{\tau}\right)^2\right],$$

where $\dot{E}_0$, t_0, and τ are parameters (t_0 is the time of the peak, and τ is the pulse length at half the power maximum). In the experiments, measurements of the energy of the ions collected by the collector, converted into numbers corresponding to the entire sphere, yielded an estimate of the total absorbed laser energy: $E_0 \approx 300–350$ J. On this basis we selected a value of $\dot{E}_0$. The parameter τ was varied. The target was a glass shell 296 μm in radius and 1.1 μm thick filled with gaseous DT to an initial density of $4.64 \cdot 10^{-4}$ g/cm³. Table I shows the calculated values of the target parameters at the time of maximum compression for the following cases:
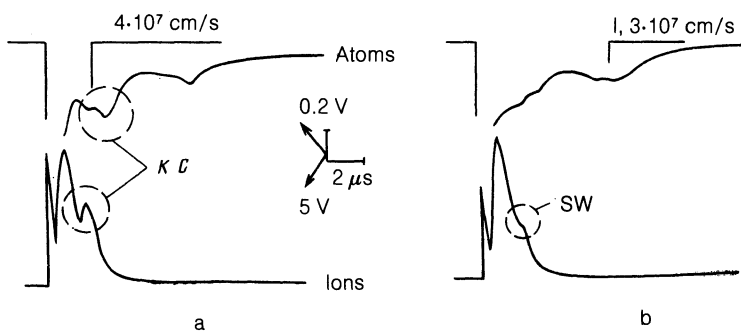

FIG. 2. Oscilloscope traces of the output signals from the ion collector and the neutral-particle detector. a: Nonuniform irradiation of a SiO₂ microballoon (diameter of 615 μm, wall thickness of 1.01 μm, DT gas pressure of 2.3 atm, laser energy of 645 J, neutron yield of $1.5 \cdot 10^9$). CJ—Suggested "wake" of the "cumulative" jet. b: Use of phase plates in the laser beams (SiO₂ microballoon: 592×1.1 μm, 2.3 atm, 616 J, neutron yield of $1.5 \cdot 10^8$). SW—Suggested "wake" of the shock wave in the target corona.
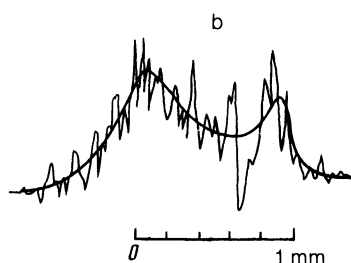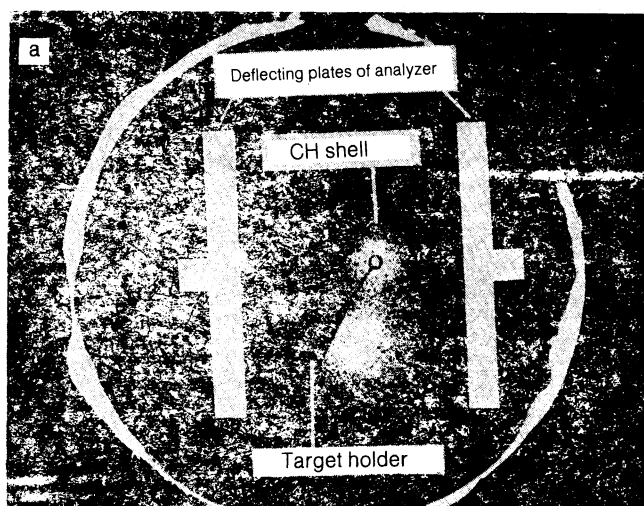
FIG. 3. a: Particle pinhole photograph of the source of neutral particles obtained during irradiation of a CH microballoon; b: Densitometer trace of the pinhole photograph in the axial cross section.

1) $t_0 = 1.2$ ns, $\tau = 0.6$ ns, $E_0 = 300$ J;

2) $t_0 = 1.2$ ns, $\tau = 0.84$ ns, $E_0 = 300$ J;

3) $t_0 = 1.2$ ns, $\tau = 0.84$ ns, $E_0 = 350$ J.

In case 2, the temporal shape of the pulse is different from that in case 1, while the total energy is the same. In case 3, the pulse length and the total energy have both been changed.

In Table I, t_* is the time of maximum compression, M_* is the mass of the compressed target (the unevaporated part of the shell, with a density $\lesssim 1$ g/cm^3, along with the mass of the DT fuel) ρ_* and T_{i*} are the average values of the ion density and temperature, respectively, in the DT fuel at the time of maximum compression, N_* is the neutron yield at this instant, and ρ_{sh} and T_{sh} are the average values of the

density and temperature of the compressed shell.

With increasing pulse length (version 2), there is a decrease in the laser flux density incident on the target. Correspondingly, the velocity of the shell and the relative amount of mass which has evaporated decrease. As a result, the temperature and the neutron yield decrease slightly, but the density of the compressed fuel and the shell increases.

After the collapse of the target, with all the compressed matter ionized and heated essentially completely, the expansion begins, and there is a partial recombination of ions of silicon, oxygen, and also deuterium and tritium. The ion composition was calculated in the approximation of an average ion charge for each component, through the use of[17]

$$\frac{dZ_k}{dt} = Z_k \, (v_{im}^{(k)} - v_{ph}^{(k)} - v_t^{(k)}), \qquad (1)$$

where Z_k is the average charge of the ion of component k (silicon, oxygen, etc.), $v_{im}^{(k)}$ is the rate of ionization by electron impact, and $v_{ph}^{(k)}$ and $v_t^{(k)}$ are the rates of photorecombination and ternary recombination. The functions $v_{im}^{(k)}$, $v_{ph}^{(k)}$, and $v_t^{(k)}$ are given in Ref. 17 [see Eq. (39) of that paper]. Calculations of the degree of ionization of the laser-target material on the basis of more-accurate models did not yield significantly different results.[18]

Velocity distributions of the neutral atoms were obtained in the calculations (in versions 1, 2, and 3) at the time $t = 10$ ns. To pursue the calculations to times $1-10\,\mu s$ would have been extremely time-consuming without being of fundamental importance, since the particles undergo essentially no collisions in the low-density expanding plasma, and a "quenching" effect[19] is seen; i.e., the charge of the ions remains constant ($Z = $ const). Figure 4 shows distributions of the density ρ, the electron temperature T_e, and the effective charge Z over the mass of the target at the time $t = 10$ ns. We do indeed find a plasma density $\rho \lesssim 10^{-4}$ g/cm^3 and a temperature $T_e \approx 3-5$ eV. In this case the time scales of the recombination of the ions of silicon, oxygen, and hydrogen are greater than $1\,\mu s$, and they increase rapidly as the medium expands (at a velocity ~ 100 km/s). The atoms and ions take $\approx 1-10\,\mu s$ to reach the collector.

It can be seen from these results that in the Vulcan experiments the neutral component of the expanding matter is only a few percent of the total compressed mass ($\sim 10^{-8}$ g) and is basically associated with the DT fuel. These results differ from the results of experiments carried out at the Del'-fin installation,[10] where the mass of neutral atoms was roughly equal to the total mass of the compressed target. The reason for this difference is that in the Vulcan experiments the laser intensity was higher, the shell masses were smaller, and the second harmonic was used.

TABLE I.

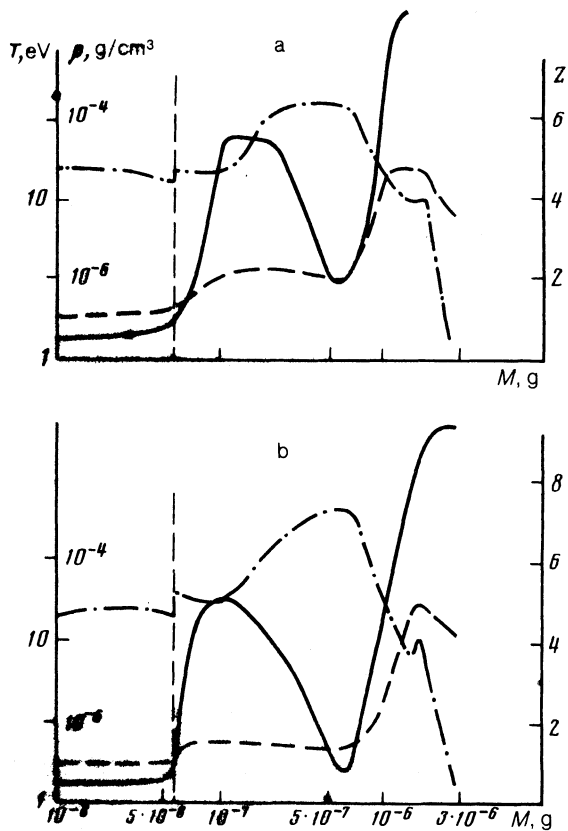|	E_0/τ, J/ns	t_*, ns	M_*, μg	ρ_{sh}, g/cm^3	T_{sh}, keV	ρ_*, g/cm^3	T_{i*}, keV	N_*
1	300/0,6	2,23	0,805	6,3	0,327	1,16	1,72	$4,6 \cdot 10^9$
2	300/0,84	2,31	0,93	15,0	0,246	1,85	1,4	$2,4 \cdot 10^9$
3	350/0,84	2,16	0,805	10,6	0,335	1,77	1,62	$5,4 \cdot 10^9$

FIG. 4. Distributions of the density ρ (dot-dashed line), the electron temperature T (dashed line), and the effective charge Z (solid line) over the mass of the shell obtained at the time $t = 10$ ns for (a) version 1 and (b) version 2. The vertical dashed line shows the shell-fuel boundary.

DISCUSSION OF EXPERIMENTAL RESULTS

In the experiments, the velocity distribution of the atoms can be found from[7]

$$\frac{dN}{dv} = L I_{se}/(k e \gamma_{se} v^2 \Omega), \qquad (2)$$

where I_{se} is the current from the electron multiplier, with a gain k and a secondary-emission yield γ_{se}; L is the distance to the target; and Ω is the solid angle. Information on the calibration curve $\gamma_{se}(v)$ is important for interpreting the results. The particle pinhole photographs were crucial in this connection. We first worked from the recorded images to calculate the density of the microchannels which were illuminated (for the case corresponding to Fig. 3, this density was 50 mm^{-2} in the target region). These results were used along with the results of Ref. 20 to approximate the function $\gamma_{se}(v) \sim v^2$. In addition, the possibility of a contribution of slow atoms from the target material was taken into consideration in the analysis of the oscilloscope traces obtained in the experiments with small targets and a high laser energy.

Figure 5 shows distributions of the slow atoms ($v \sim 2.5 \cdot 10^7$ cm/s) in experiments with nonuniform irradiation of the targets. We see from this figure that the velocity distributions of the atoms are similar in experiments in which the laser pulse and the target had approximately the same parameter values. In all the shots reported here, the neutron yield exceeded 10^9 [the range was $(1.5–3) \cdot 10^9$]. The experimental data can be approximated satisfactorily by the function

$$dN/dv = N_0 \exp(-v/v_0), \qquad (3)$$

where $N_0 = 10^5$ (sr·cm/s)$^{-1}$ and $v_0 = 0.3 \cdot 10^7$ cm/s.

Under the assumption that the atoms moving at velocities $(1–2) \cdot 10^7$ cm/s constitute matter of the compressed shell (with a mass $M_* \approx 0.1 M_0$), we estimate the relative number of atoms to be $\sim 10^{-4}–10^{-5}$. In other words, the ions do not recombine to a neutral state during the movement of the shell. This result is attributed to the high temperature (more than 100 eV) and the relatively low density (below 20 g/cm^3) at the time of collapse. The increase in the number of atoms for $v < 10^7$ cm/s is apparently due to atoms of the target holder. This suggestion is in accordance with Fig. 6, which shows data with more atoms at velocities $v < 10^7$ cm/s. Shots of this sort are characterized by either a high laser energy or a small target diameter, i.e., by conditions such that an effect of the target is most likely. In addi-
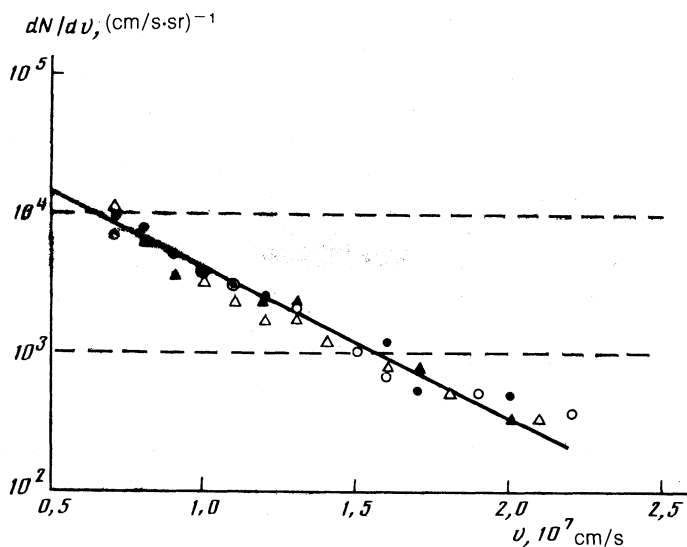

FIG. 5. Typical velocity distributions of the atoms in the case of nonuniform irradiation of an SiO$_2$ target. $\triangle$—Diameter of 610 μm, thickness of 1.0 μm, laser energy of 765 J, neutron yield of $3 \cdot 10^9$; $\bigcirc$—659$\times$0.8 μm, 654 J, $1.5 \cdot 10^9$; $\bigcirc$—599$\times$1.06 μm, 619 J, $2 \cdot 10^9$; $\triangle$—615$\times$1.01 μm, 645 J, $1.5 \cdot 10^9$.
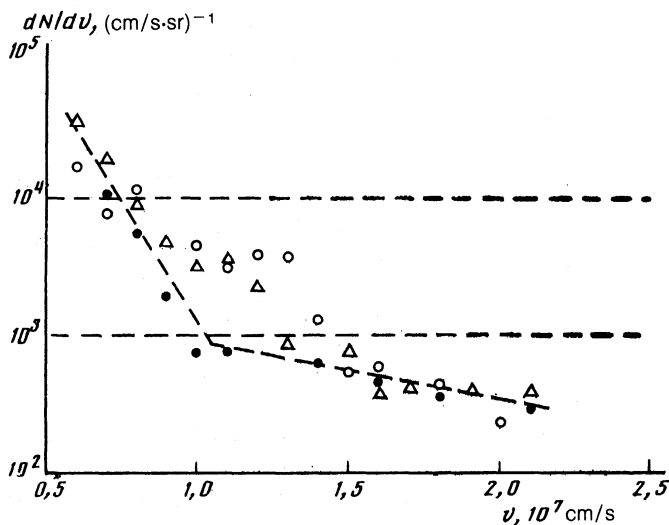
dN/dv, $(\text{cm·s·sr})^{-1}$

FIG. 6. Velocity distributions of atoms in shots with possible effect of emission from the target holder. O—SiO_2, $572\times2.1\,\mu\text{m}$, 750 J, empty shell; ●—$SiO_2$, $497\times1.2\,\mu\text{m}$, 770 J, 1.5×10^8; △—CH, $298\times13\,\mu\text{m}$, 293 J.

tion, the increase in the number of slow atoms may be due to a mixing of the shell and fuel material during the slowing stage.

Figure 7 shows velocity distributions of the atoms in experiments with a smooth irradiation. The shell collapse velocity (determined from the results of x-ray streak photography) is lower, and the neutron yield is substantially lower, $\sim(0.2-1.5)\cdot10^8$.

All the results in Fig. 7 show that the number of atoms with velocities $v<1\cdot10^7$ cm/s decreases with a decrease in the local value of the laser flux density on the target. This result can be attributed to a weaker effect of the atoms from the target holder and also to more symmetric compression of the DT gas. At velocities $v>2\cdot10^7$ cm/s, the number of atoms is also lower than in the case of a nonuniform irradiation. This fact can be explained on the basis of the focusing

dN/dv, $(\text{cm·s·sr})^{-1}$

FIG. 7. Velocity distributions of atoms in experiments with phase plates in the laser beams (SiO_2 shells). O—$593\times1.3\,\mu\text{m}$, 546 J, $2.1\cdot10^7$; ●—$587\times1.2\,\mu\text{m}$, 638 J, $3.9\cdot10^7$; ▲—$598\times0.77\,\mu\text{m}$, 418 J, $1\cdot10^8$; △—$592\times1.1\,\mu\text{m}$, 616 J, $1.5\cdot10^8$; solid line—approximation by a model of a gaseous sphere.

geometry: During smooth irradiation, the plasma corona moving toward the observer has a higher temperature (and a higher ion charge) than in the case of a nonuniform irradiation. A second factor which tends to increase the number of fast atoms [and also the number of ions with velocities $(3-4)\cdot10^7$ cm/s] might be a cumulating jet along the observation direction. A similar effect was detected in Ref. 21.

Comparison of Figs. 5 and 7 leads to the conclusion that neutral atoms of the residual shell mass can be observed, and the shape of the velocity distribution can be reconstructed, in the case of a smooth irradiation of the target. This smooth irradiation is achieved by placing matrix phase plates in the laser beams. During nonuniform irradiation of the target, the observation direction corresponds to a cold region, as can be seen from the increased number of fast atoms, which arise during recombination of low-charge ions of the plasma corona, and also from the cumulating jet which is formed. This effect can also be seen in the increase in the number of slow atoms which correspond to regions of a pronounced mixing of the target and which are emitted by the target holder. It is thus exceedingly difficult to distinguish the signal representing the residual-mass atoms.

The double-hump structure of the current pulse of the ions and the atoms in Fig. 2a can be attributed to the onset of multidimensional effects during the asymmetric heating and compression of the shell. The appearance of the additional peak of fast atoms in the current can be explained qualitatively in the following way. Consider Fig. 8, which is a schematic diagram of the target irradiation conditions in this experiment. Since the light intensity and the pressure on the unevaporated shell are higher at the axes of the beams than at the bisector of the angle ($\theta\approx30°$), these regions of the shell move more rapidly. They form "convex fronts" of shock waves in the DT gas. After the shock waves are reflected from the center, the temperature and therefore the sound velocity in the DT plasma increase sharply. The pressure in the fuel tends to become uniform. This tendency could in principle lead to the formation of a cumulating jet along the bisector. As a result, some of the cold, unevaporated shell and the DT plasma at $\theta=30°$ acquire additional momentum. This effect might explain the first peak (Fig. 2a). The second peak consists of the remainders of the fuel and the

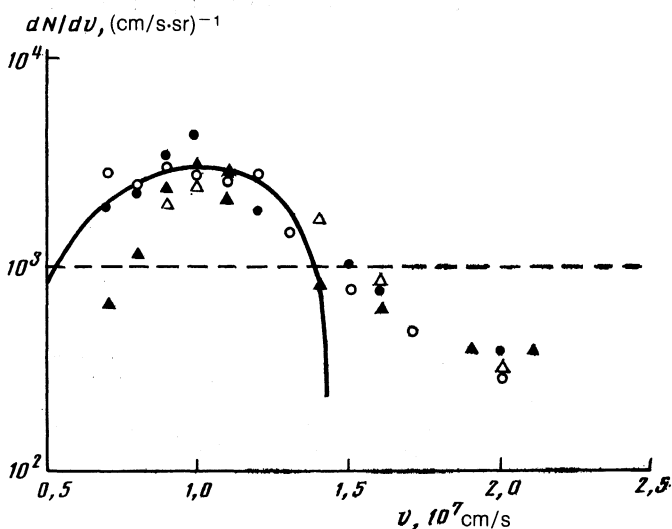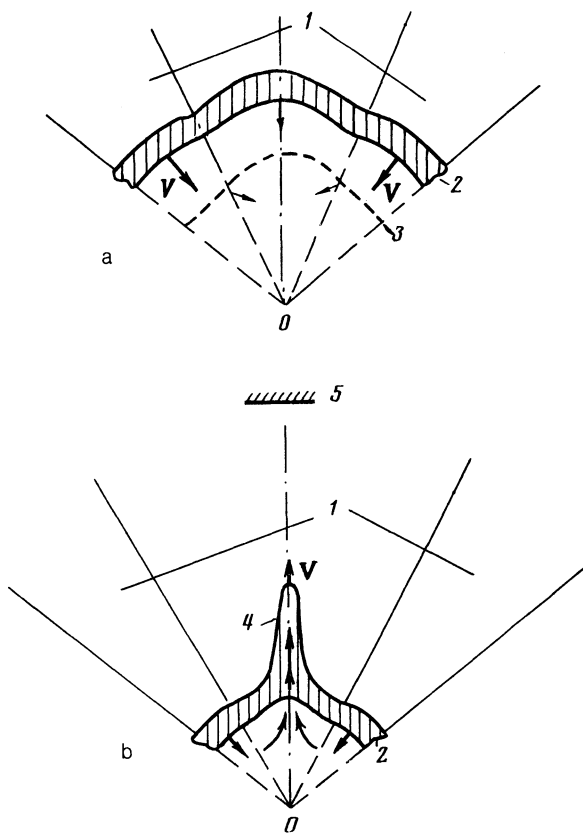FIG. 8. Formation of a jet along the bisector of the angle between the optical axes of incident laser beams (the total angle at 60°). a: Initial stage of process. 1—Laser beams; 2—unevaporated shell; 3—front of converging shock wave (shown by the dashed line). b: Formation of jet. 4—Jet; 5—neutral-particle detector.
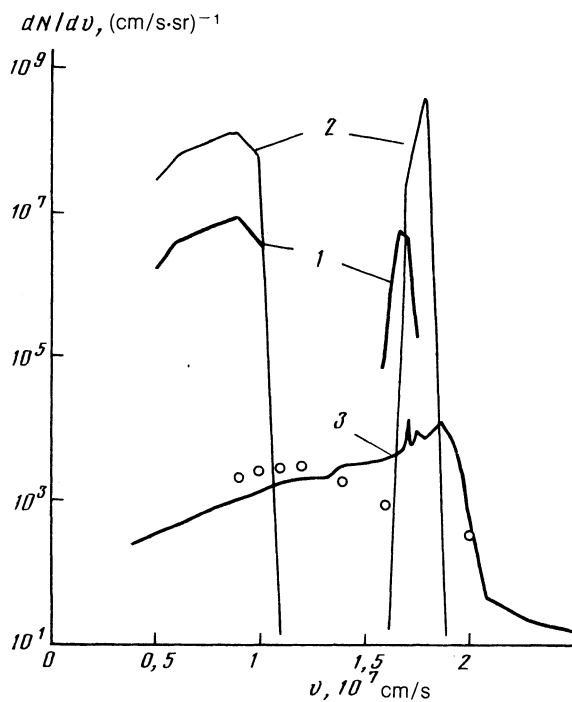

FIG. 9. Velocity distribution of atoms at the time $t = 10$ ns found in calculation versions 1 and 2 (lines 1 and 2, respectively). Mixing was ignored in these calculations. Line 3—Spectrum of atoms found in a calculation with mixing, for version 2 of the parameters of the laser pulse. The points are experimental data corresponding to approximately equal values of the parameters of the laser pulse and of the target.

shell which have undergone a collision at the center and which have arrived at the collector. A quantitative description of this effect will require two-dimensional calculations, for which an appropriate mathematical model is presently being developed.

COMPARISON OF THE NUMERICAL SIMULATION WITH EXPERIMENT

The velocity distribution of the neutral atoms found experimentally (Fig. 7) is broader than the calculated distribution (curves 1 and 2 in Fig. 9), although the velocity ranges are the same. This result appears to indicate that intense mixing of the shell and fuel material occurs during the slowing of the shell and then in the initial stage of the expansion (in these stages, the density gradient and the pressure gradient are antiparallel; i.e., the conditions favor the onset of a Rayleigh–Taylor instability).

To incorporate the turbulent mixing in the one-dimensional calculations, we used the following simplified model. We assumed that a fraction c of the unevaporated shell mass (cM_{unevap}) mixed with the fuel (M_{DT}) in the stage in which the shell was slowed down by the shock waves reflected from the center. We assumed that at the time t_M (the value $t_M = 2$ ns was used in the calculations) the mixed material was distributed uniformly and was at rest:

$$\rho_m = \frac{M_m}{\frac{4}{3}\pi R_m^3},\tag{4}$$

$$E_m = (1 + \overline{Z}_m(T_m))C_V M_m T_m.\tag{5}$$

Here C_V is the heat capacity of the ions of the mixture; $M_M = cM_{unevap} + M_{DT}$ is the mass of the mixed material; and E_M, T_M, ρ_M, and $\overline{Z}_M$ are respectively the internal energy, temperature, density, and average charge of this material. The values of T_M and $\overline{Z}_M$ were found from (5) and the Saha condition $Z_m = Z_m(\rho_m T_m)$. For $t > t_M$, the target was compressed for an even longer time and then began to expand. The total relative number of neutral atoms was lower than in the preceding versions, and the spectra were broader. In the case $\overline{Z} > 1$ the number of neutral atoms in a cell, n_k, was found from

$$n_k = n_{k0} \exp(-(\overline{Z}_k/\Delta)^2), \quad \Delta = \left[\frac{2Z_k}{I_k/T}\right]^{\frac{1}{2}}.\tag{6}$$

Here n_k and n_{k0} are the number of neutral atoms and the total number of ions of species k (Si, O) in the computation cell, and $I_k/T \approx 5$.

Curve 3 in Fig. 9 shows the spectra of neutral particles found in the second version of the calculation with allowance for mixing ($c = 0.68$). The points are experimental data.

We proposed a simple model in Ref. 10 for describing the expansion of a sphere of recombining plasma into vacuum. The problem was solved numerically. It was found that incorporating plasma recombination had no great effect on the dynamics of the plasma, so in a first approximation it was

legitimate to use a self-similar solution for the adiabatic expansion of a gaseous sphere into vacuum:[19]

$$\frac{dN}{dv} = \frac{N_0}{v_m}\left(\frac{v}{v_m}\right)^2\left[1-\left(\frac{v}{v_m}\right)^2\right]^{1/(\gamma-1)}.$$ (7)

Here v_m is the maximum velocity, and γ is the adiabatic index. The values of N_0 and v_m can be found from the results of the one-dimensional calculations (at the time at which the shell begins to be slowed by the fuel), or they can be found from experimental data. Figure 7 shows an approximation of the experimental data by expression (7).

In contrast with the model of a gaseous sphere expanding into vacuum, however, the expansion of the compressed matter occurs into the atmosphere of the plasma corona. In Figs. 4a and 4b we see humps in the low-density region which are associated with the propagation of shock waves in the corona. In other words, part of the energy is carried off from the cold, dense plasma by these waves.

Despite the low density of the plasma corona, the expanding shell of compressed matter is slowed down. As a result, its final velocity is noticeably lower than the maximum collapse velocity u_{sh}. At the same time, the shock wave accelerates the ions in the target corona.

The slowing of the shell can be studied with the help of a simplified model of the interaction of two objects with initial masses M_{sh} (the shell) and M_p (the plasma involved in the interaction), with respective velocities u_{sh} and v_{p1} (for the plasma, v_{p1} is the velocity of the center of mass). The impulse acquired by the plasma is

$$\Delta I = M_{sh}(u_{sh}-u_n) = M_p(v_{pe}-v_{p1}),$$ (8)

where u_n is the velocity of the shell after the slowing by the plasma (this is the velocity of the center of mass of the neutrals), and v_{p1} is the velocity of the accelerated plasma. Using $v_{p1} \approx C_{sh}$, where the right side is the sound velocity in the plasma, we find

$$v_{p^2} = C_{sh} + \frac{M_{sh}}{M_p}U_n\left(\frac{u_{sh}}{u_n}-1\right).$$ (9)

Substituting (9) into the condition for conservation of kinetic energy in the course of an elastic collision, we can determine the mass and velocity of the plasma (because of the high temperature of the coronal plasma in the initial stage of the expansion, the assumption of an "elastic" collision is valid in a first approximation):

$$M_p = \frac{u_{sh}-u_n}{u_{sh}+u_n-2C_{sh}}M_{sh},$$ (10)

$$v_{p2} = u_{sh}+u_n-C_{sh}.$$ (11)

In these experiments, the collapse velocity found from the streak x-ray pinhole photographs was $u_{sh} = (2.5-3)\cdot 10^7$ cm/s. As we mentioned earlier, the average velocity of the atoms was $u_n \approx 1\cdot 10^7$ cm/s. Taking the sound velocity to be $C_{sh} \approx (1-1.5)\cdot 10^7$ cm/s, which is a typical value for these experimental conditions, we find $v_{p2} = (2-3)\cdot 10^7$ cm/s and $M_p = (0.5-1)M_s$.

The impulse transferred to the plasma propagates along the decaying density profile. As a result, the discontinuity may be accelerated to slightly higher velocities.[19,22] It is possible that this discontinuity was detected by the ion and atom collectors (Fig. 2b), i.e., that it represented the "fast" atoms with velocities of $(3-4)\cdot 10^7$ cm/s. According to (11), the velocity of the shock wave in the corona, v_{p2}, increases with decreasing C_{sh} (this increase occurs in the cold plasma in the observation direction) and becomes considerably higher than u_n (in certain cases it may also be higher than u_{sh}). The number of neutral atoms in the hotter plasma decreases simultaneously.

CONCLUSION

Analysis of the velocity distributions of the atoms and analysis of the particle pinhole photographs make it possible to distinguish the various components of the emission source. In particular, in the case of nonuniform irradiation of the target the recombined low-charge ions of the plasma corona of the cold region and the emission of holder atoms become extremely important. They complicate a study of the atoms of the residual mass of the shell.

The presence of a double-hump structure in the current pulse of the ions and neutral atoms in the case of an asymmetric irradiation suggest the formation of a cumulating jet. During smooth irradiation of the target, it is possible to achieve a qualitative agreement between the calculated and experimental spectra. For example, the peaks in the distributions of neutral atoms coincide, as do the positions of the shock front in the plasma corona. The fact that the experimental spectra are broader than the calculated spectra indicates the onset of turbulent mixing of the fuel and the shell during the stage of slowing and expansion.

There are wider opportunities for diagnostics of the compressed target in experiments on ultradense ablative compression of relatively thick microballoons, with a pulse length shorter than or equal to the target collapse time.

[1] N. G. Basov, Yu. A. Zakharenkov, N. N. Sorev et al., "Heating and compression of laser-irradiated fusion targets," in Scientific and Technological Progress, VINITI, Moscow, 1982.

[2] Yu. V. Afanas'ev and V. B. Rozanov, Zh. Eksp. Teor. Fiz. 62, 247 (1972) [Sov. Phys. JETP 35, 133 (1972)].

[3] Yu. A. Bykovskii, N. N. Degtyarenko, V. S. Fetisov et al., Zh. Eksp. Teor. Fiz. 44, 73 (1974) [sic].

[4] R. R. Goforth and P. Hammerling, J. Appl. Phys. 47, 3918 (1976).

[5] G. J. Tallents, Plasma Phys. 22, 709 (1980).

[6] Yu. A. Bykovskii and S. M. Sil'nov, Fiz. Plazmy 15, 1091 (1989) [Sov. J. Plasma Phys. 15, 632 (1989)].

[7] N. G. Basov, Yu. A. Zakharenkov, A. A. Rupasov et al., Diagnostics of Dense Plasmas, Nauka, Moscow, 1989.

[8] N. G. Basov, P. P. Volosevich, E. G. Gamalii et al., Zh. Eksp. Teor. Fiz. 78, 420 (1980) [Sov. Phys. JETP 51, 212 (1980)].

[9] S. Denus, J. Farny, M. Grudzien et al., Laser and Part. Beams 4, 507 (1986).

[10] Yu. A. Zakharenkov, A. A. Karnaukhov, V. Ya. Karpov et al., Fiz. Plazmy 14, 623 (1988) [Sov. J. Plasma Phys. 14, 367 (1988)].

[11] C. N. Danson, Ann. Rep. Las. Fac. Commit. Ral-89-045, 133 (1989).

[12] M. J. Lamb, M. Savage, P. Fews et al., in Twentieth European Conference on Laser Interactions with Matter, Schliersee, 1990.

[13] P. A. Fews, M. J. Lamb, and M. Savage, Ann. Rep. Las. Fac. Commit. Ral-90026, 36 (1990).

[14] Z. Ahmad, A. A. Erokhin, Yu. A. Zakharenkov et al., Pis'ma Zh. Eksp. Teor. Fiz. 51, 553 (1990) [JETP Lett. 51, 626 (1990)].

[15] A. A. Erokhin, Yu. A. Zakharenkov, A. A. Karnaukhov et al., Fiz. Plazmy 15, 1076 (1989) [Sov. J. Plasma Phys. 15, 624 (1989)].

[16] I. V. Zmitrenko, V. Ya. Karpov, A. P. Fadeev et al., in Questions of Atomic Science and Engineering. Methods and Programs for Numerical Solution of Problems of Mathematical Physics, Vol. 2, 1983, p. 38.

[17] Yu. V. Afanas'ev, E. G. Gamalii, and V. B. Rozanov, Tr. FIAN 134, 10 (1982).

635   Sov. Phys. JETP 73 (4), October 1991

Ahmad et al.   635

[18] B. N. Bazylev, F. N. Borovik, G. A. Vergunova *et al.*, Kvantovaya Elektron. (Moscow) **13**, 1981 (1986) [Sov. J. Quantum Electron. **16**, 1308 (1986)].

[19] Ya. B. Zel'dovich and Yu. P. Raizer, *Physics of Shock Waves and High-Temperature Hydrodynamic Phenomena*, Nauka, Moscow, 1966 (Academic, New York, 1966).

[20] A. A. Golubev, Yu. A. Zakharenkov, A. A. Karnaukhov *et al.*, Kvant. Elektron. (Moscow) **15**, 630 (1988) [Sov. J. Quantum Electron. **18**, 403 (1988)].

[21] E. F. Gabl, B. H. Failor, C. J. Armentrout *et al.*, Phys. Rev. Lett. **63**, 2737 (1989).

[22] Yu. V. Afanas'ev, N. G. Basov, B. L. Vasin *et al.*, Zh. Eksp. Teor. Fiz. **77**, 2539 (1979) [Sov. Phys. JETP **50**, 1229 (1979)].

Translated by D. Parsons

636   Sov. Phys. JETP **73** (4), October 1991

Ahmad *et al.*   636